INTERNATIONAL JOURNAL FOR NUMERICAL METHODS IN FLUIDS, VOL. 16, 967–988 (1993)

TRANSIENT SIMULATION OF 2–3D STRATIFIED AND INTERMITTENT TWO-PHASE FLOWS. PART II: APPLICATIONS

RANDI MOE

Institutt for energiteknikk, P.O. Box 40, 2007 Kjeller, Norway

SUMMARY

In this paper a new type of transient multidimensional two-fluid model has been applied to simulate intermittent or slug flow problems. Three different approaches to modelling interfacial friction, including an interfacial tracking scheme, have been investigated. The numerial method is based on an implicit finite difference scheme, solved directly in two steps applying a separate equation for the pressure. 2D predictions of Taylor bubble propagation in horizontal and inclined channels have been compared with experimental data and analytical solutions. The 2D model has also been applied to investigate a number of special phenomena in slug flow, including slug initiation, bubble turning in downflow and the bubble centring process at large liquid flow rates.

KEY WORDS. Transient 2–3D simulation Two-phase flows Intermittent flows Taylor bubbles

1. INTRODUCTION

Details of multiphase flow presently have to be studied through extensive experiments, as only in special cases 2–3D models can be applied with confidence. For two-phase flow, however, at least three general purpose codes (FLUENT, FLOW-3D and PHOENICS) are available, as well as a series of more problem-oriented models. All these apply finite difference schemes, based mainly on the work of Patankar and Spalding, and are generally limited to dispersed flows or particle tracking. A different approach to steady 2–3 modelling of bubbly two-phase flow has recently been proposed by Antal *et al.*,[1] based on a Galerkin type of finite element method.

Modelling separated or stratified flow in general is complicated by two factors: the interface location and the interfacial wave pattern. Both are physical manifestations of the particular two-phase flow itself, and must be treated as integral parts of any model of the flow by determining, for example, interfacial friction and overall pressure drop. Hirt and Nichols[2] proposed an algorithm to track free surfaces or interfaces between two fluids. Their model is, however, a modified single-phase description, with explicit updating of interface locations.

In this work a 2–3D transient model proposed by Moe and Bendiksen[3] has been applied. Closure laws are still not general, but are focused on separated or stratified flow problems. Three different approaches to modelling interfacial friction, including a volume of fluid donor–acceptor interfacial friction scheme, have been investigated. The numerical scheme is based on an extension of the one-dimensional models of Bendiksen *et al.*[4,13] A 'volume' equation is applied for the pressure, allowing a direct two-step solution procedure. First the pressure and velocities are

0271–2091/93/110967–22$16.00

Received June 1992
Revised January 1993

solved implicitly from the volume and momentum equations, and then the specific masses are solved from the continuity equations. These linearized equations sets are solved directly by applying a Gaussian band solver and avoiding an iterative solution procedure.

Predictions of Taylor bubble propagation in horizontal and inclined channels have been compared with experimental data and analytical solutions. The model is also shown to simulate a number of different special phenomena of slug flow, including slug initiation, Taylor bubble turning in downflow, and the process of Taylor bubble centring at high liquid flow rates.

2. PHYSICAL MODEL

2.1. Basic conservation equations

The model of Moe and Bendiksen[3] was developed considering the local instantaneous two-fluid formulation of each phase, imposing appropriate averaging and thus obtaining a set of time- and space-averaged conservation equations. In the averaging process a single (fluctuating) time or spatial scale has been assumed, important characteristics of the flow field are lost and must be reintroduced into the model through appropriate closure laws. A common pressure field is applied, mass transfer between the phases has been neglected, and a constant-temperature field assumed. The mass and momentum balances for each k ($k=\ell$, g) are then expressed as follows:

Conservation of mass

$$\frac{\partial}{\partial t}(\alpha_k \rho_k)+\nabla\cdot(\alpha_k \rho_k \mathbf{u}_k)=0. \tag{1}$$

Conservation of momentum

$$\frac{\partial}{\partial t}(\alpha_k \rho_k \mathbf{u}_k)+\nabla\cdot(\alpha_k \rho_k \mathbf{u}_k \mathbf{u}_k)=-\nabla(\alpha_k p_k)+\alpha_k \rho_k \mathbf{g}+\nabla\cdot[\alpha_k(\tau_k+\tau_k^{\mathrm{T}})]+\mathbf{M}_k \tag{2}$$

and the relation

$$\alpha_{\mathrm{g}}+\alpha_\ell=1, \tag{3}$$

where $\mathbf{u}_k$ denotes the velocity, p the pressure, ρ_k the density, τ_k the viscous shear stress, τ_k^{T} the turbulent flux, $\mathbf{g}$ the acceleration due to gravity and α_k the volumetric fraction of phase k. The term $\mathbf{M}_k$ represents the interfacial momentum transfer.

2.2. Closure relations

Separated and intermittent flow regime description. This work is focused on flows with relatively large separating interfaces between the fluids, such as elongated bubbles. The interfacial momentum transfer, $\mathbf{M}_k$, is expressed as

$$\mathbf{M}_k=\mathbf{M}_k^{\mathrm{d}}+\mathrm{p}_{ki}\nabla\alpha_k-\tau_{ki}\nabla\alpha_k-\tau_{ki}^{\mathrm{T}}\nabla\alpha_k, \tag{4}$$

when omitting mass transfer between the phases. This relation and the momentum equations can be simplified further by neglecting surface tension and assuming a common pressure field for the two phases, as discussed by Moe and Bendiksen.[3] For separated flows the interfacial momentum transfer is due to normal and tangential stress (drag), and to the level of turbulence at the interface.

For an ordinary two-fluid model the ratio between the phases is given by the volumetric fractions, α_g, α_ℓ, of each phase. The position of the interface itself has to be specified in terms of

mean quantities. The interface in gravity-dominated flows is often assumed to be located where the volumetric fraction is 0·5, as suggested by Liu and Spalding.[5] Its position is then obtained simply by plotting the contour line of $\alpha_g = \alpha_\ell = 0{\cdot}5$. This approach will, however, lead to a strong diffusion of the interface.

An improved method to track the interface between two fluids was proposed by Hirt and Nichols.[2] Their 'volume of fluid' (VOF) method consists of a set of single-phase equations in addition to a fractional volume of fluid function, F. The value of this function is unity or zero at any point occupied by either of the fluids. When applying the function F in a computational mesh (see Figure 1), the averaged value of F in a cell is equal to the fractional volume of the cell occupied by the fluids. The function F is also used to locate the fluids in the cell. This information is used together with the donor–acceptor method described by Johnson[6] to calculate the mass flux with a minimal diffusion of the interface.

The essential idea of the donor–acceptor method is to use information on the interface orientation in the upstream cell to calculate the flux across each cell boundary in the downstream direction. The orientation of the interface has to be approached by a step function; see Figure 2. The accuracy of this method depends on the accuracy in predicting the interface location within a cell, as well as the applied mesh and the time step.

In the VOF method outlined above, a single set of momentum equations describes the flow field. The two fluids in a cell are constrained to move with equal velocities. In reality, however, for two fluids of different properties (density, viscosity) a strong shear can occur close to the interface, causing quite different phase velocities.

By applying the donor–acceptor method in a two-fluid model, one should be able to calculate the velocity close to the interface more accurately. However, one has to solve two sets of equations in the single-phase domains.

Interface tracking. The proposed two-fluid model has been used to test an interface tracking scheme, based on the Donor–Acceptor method and also to investigate the influence of different interfacial friction models in separated flows.

Implementation of the interface tracking method depends on the numerical scheme and solution procedure applied. The basic idea is to modify the mass flux terms in the conservation equations. In a staggered mesh (finite difference scheme), mass flux terms are normally defined as products of a phase velocity defined at the cell boundary and a mean mass, without taking into account the precise distribution (interface orientation) of the two fluids. This will thus lead to a diffusion of sharp interfaces.

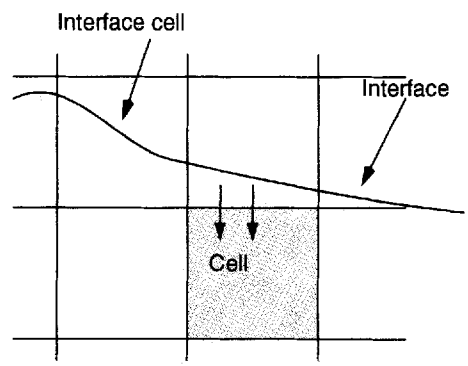

Figure 1. A view of the interface in a computational mesh

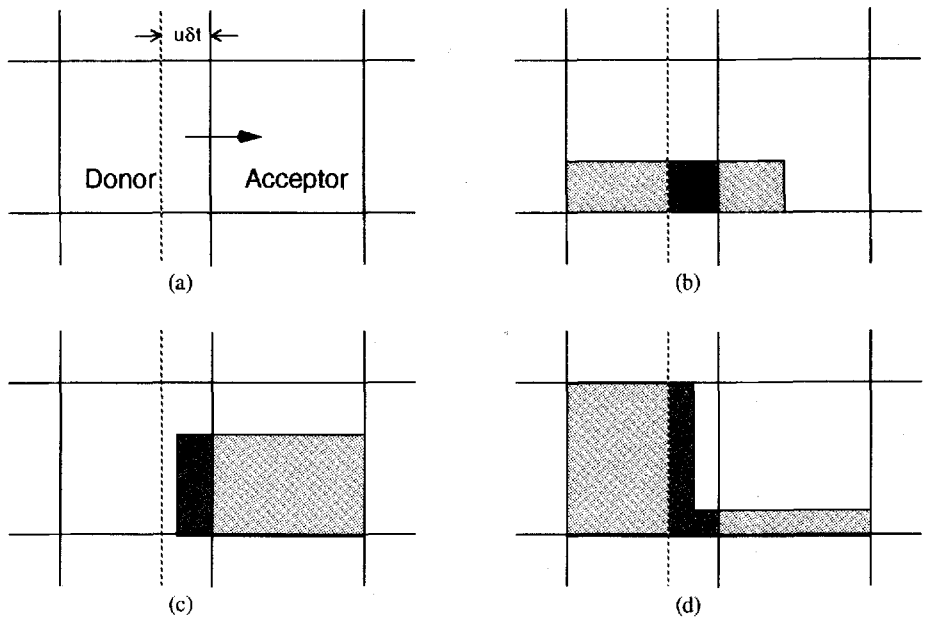

Figure 2. Examples of interface shapes used in the advection of fluids. The donor–acceptor arrangement is shown in (a), where the dashed line indicates the left boundary of the total volume being advected. The cross-hatched regions shown in (b)–(d) are the actual amounts of volume fluxed (Hirt and Nichols[2])

Imposing an interface tracking method modifies the mass flux terms according to the location of the two fluids inside a spatial mesh. A more detailed description of the applied method will be presented in connection with the solution procedure and numerical scheme.

Interfacial friction. According to Moe and Bendiksen,[3] under certain relevant assumptions the jump conditions for the momentum balance reduce to the skin drag force only:

$$\mathbf{M}_\ell = -\mathbf{M}_\mathrm{g} = \mathbf{M}_k^\mathrm{d}. \tag{5}$$

Interfacial friction is modelled through an extension of the method applied in one-dimensional models (e.g. Bendiksen *et al.*[4]). Assuming the drag force to be proportional to the velocity difference squared between the phases, this force can be expressed in Cartesian co-ordinates as

$$\begin{aligned} \mathbf{M}_\ell^x &= F_\mathrm{i}^x |u_r| u_r, \qquad F_\mathrm{i}^x = \frac{1}{2}\rho_\mathrm{g}\lambda_\mathrm{i}^x \frac{S_\mathrm{i}}{A}, \\ \mathbf{M}_\ell^y &= F_\mathrm{i}^y |v_r| v_r, \qquad F_\mathrm{i}^y = \frac{1}{2}\rho_\mathrm{g}\lambda_\mathrm{i}^y \frac{S_\mathrm{i}}{A}, \end{aligned} \tag{6}$$

where

$$\begin{aligned} u_r &= u_\ell - u_\mathrm{g}, \\ v_r &= v_\ell - v_\mathrm{g}, \end{aligned} \tag{7}$$

The interfacial perimeter, S_i, denotes the area of the interface and A is the volume of the actual flowfield. Although a simplification, the drag force (6) is quite general, and incorporates a variety of different physical interfacial conditions. Several types of interfacial friction factors (λ_i) have

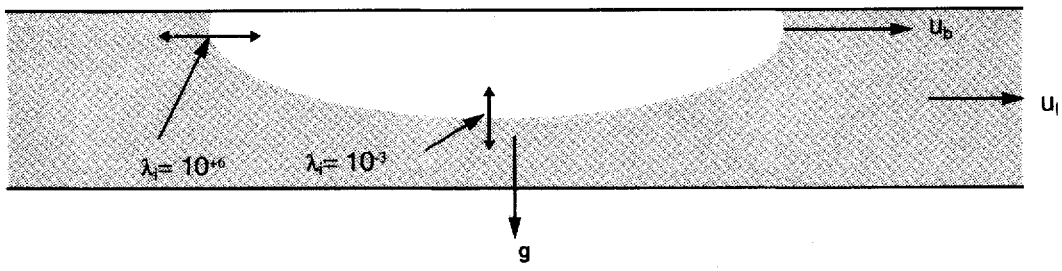

Figure 3. Elongated bubble flow

been investigated. A modification of the Wallis[7] formula,

$$\lambda_i^x = \lambda_i^y = 0{\cdot}02\ (1 + 75h_\ell), \tag{8}$$

where h_ℓ is the liquid hold-up, has been found to describe stratified or annular flows quite well. This interfacial condition applies to stratified or annular flows and gives a linear increase in the interfacial drag with increasing liquid hold-up.

An extreme approach to modelling interfacial friction is to impose a very strong coupling in the main (axial) flow direction and no interaction in the transverse direction

$$\lambda_i^y = 10^{-3}, \qquad \lambda_i^x = 1{\cdot}0 \times 10^6. \tag{9}$$

Applying a strong interaction in the main flow direction is physically correct when approaching the interface in the limit, as this results in a no-slip condition. When this relation is used inside a computational mesh, it will force the velocities of the two phases to be equal 'close' to the interface. The weak coupling applied in the transverse direction is suitable for interfaces dominated by gravity. Relation (9) describes elongated bubbles in a channel or pipe very well; see Figure 3.

Shear stress modelling. On the basis of the assumption of Newtonian fluids, the average stress tensor for laminar flow is normally expressed as for single-phase flow:

$$\tau_k = \mu_k(\nabla \mathbf{u}_k + \nabla \mathbf{u}_k^*) - ((\tfrac{2}{3}\mu_k - \lambda_k)\nabla \cdot \mathbf{u}_k \Im), \tag{10}$$

where μ_k and λ_k are the viscosity and the bulk viscosity of phase k, $\Im$ is the unity tensor, and all quantities are time averaged.

For turbulent flow, neglecting possible effects due to interface fluctuations, the Reynolds stresses may be expressed as

$$\tau_k^{\mathrm{T}} = -\overline{\rho_k \mathbf{u}_k' \mathbf{u}_k'}, \tag{11}$$

where $\mathbf{u}_k'$ represents the local velocity fluctuations of phase k.

For single-phase flow the Boussinesq approach is applied to model turbulence. The effective turbulent shear stresses are replaced by the product of the mean velocity gradient and the 'turbulent viscosity', μ_{T}, which is dependent on the flow field:

$$-\overline{\rho_k \mathbf{u}_k' \mathbf{u}_k'} = \rho_k \mu_k^{\mathrm{T}}(\nabla \mathbf{u}_k + \nabla \mathbf{u}_k^* - \tfrac{2}{3}(\nabla \cdot \mathbf{u}_k \Im)). \tag{12}$$

For multiphase or two-phase flow this method cannot be adopted without further justification, as the macroscopic averaged equations contain interfaces which are no longer described separately, but through the volume fractions (α_k). The problem of turbulence in dispersed flow has been

considered by several authors. Normally, it is accounted for in the continuous phase through a modified mixing length, a k–ε or full Reynold stress model. The thesis by Ellull[8] provides a recent overview of the problem.

In our proposed model the Boussinesq approach to turbulence has been applied for each phase k:

$$\mu_{k,\text{eff}} = \mu_k + \mu_k^{\text{T}}. \tag{13}$$

The turbulent eddy viscosity (μ_k^{T}) will display spatial variations for each phase and will also be influenced by the interface. For the flow problems to be studied in this work, average flow parameters are not expected to be particularly sensitive to turbulent effects. Thus, the simple Prandtl mixing-length hypothesis has been applied as described by Moe and Bendiksen.[3]

Boundary and initial conditions. Remaining closure laws, boundary and initial conditions applied are as described by Moe and Bendiksen.[3]

2.3. *Numerical solution procedure*

Equations (1)–(3) together with the constitutive relations described above yield a set of coupled first-order non-linear partial differential equations. The tight coupling between pressure and phase velocities requires in general a simultaneous or iterative solution of the mass and momentum conservation equations. An efficient and numerically robust solution is obtained by combining the mass equation (1) into a 'volume equation', as described by Moe and Bendiksen,[3] or Bendiksen *et al.*[4]:

$$\left(\frac{\alpha_g}{\rho_g}\frac{\partial \rho_g}{\partial p} + \frac{\alpha_\ell}{\rho_\ell}\frac{\partial \rho_\ell}{\partial p}\right)\frac{\partial p}{\partial t} = -\frac{1}{\rho_g}\frac{\partial}{\partial x}(m_g u_g) - \frac{1}{r}\frac{1}{\rho_g}\frac{\partial}{\partial y}(r m_g v_g) - \frac{1}{\rho_\ell}\frac{\partial}{\partial x}(m_\ell u_\ell) - \frac{1}{r}\frac{1}{\rho_\ell}\frac{\partial}{\partial y}(r m_\ell v_\ell). \tag{14}$$

The numerical solution procedure is based on a first-order semi-implicit finite difference scheme. A staggered mesh or Arakawa C-grid has been applied. This type of grid consists of cells where velocities are defined on the boundaries and pressures and specific masses are defined inside the volumes.

A semi-implicit method resulting in a split solution procedure at each time step has been applied.[3] Required flow parameters and coefficients are updated based on the state vector (velocities, etc.) from the last time step. Velocities and pressures are then calculated from the momentum equations and the 'volume' equation, using specific masses and volume fractions from the previous time step. Under the assumption of no interfacial mass transfer, the mass equations are decoupled, and may be solved separately. When specific masses and densities are known, the volume fractions can be obtained directly from the definition ($m_k \equiv \alpha_k \rho_k$). This set of equations is, however, overdetermined as the volume relation ($\alpha_g + \alpha_\ell = 1$) also applies. The solution method may thus give rise to an error in specific volume, and an iterative volumetric correction procedure has been included at each time step.

Further details on the numerics may be found in the work of Moe and Bendiksen.[3]

Interface tracking. A first approach to track interfaces numerically in the two-fluid model has been implemented for interfaces orientated normally to the main flow direction. The original scheme is mass conserving, applying mean masses in the 'donor cell'. Modifying relevant mass fluxes, the interface tracking scheme is obtained. For the actual interface, the mass flux terms can be modified by simply applying 'forward' instead of 'backward' specific masses, as shown in Figure 4. This will significantly reduce numerical diffusion. The method is easily implemented in the finite difference equations.

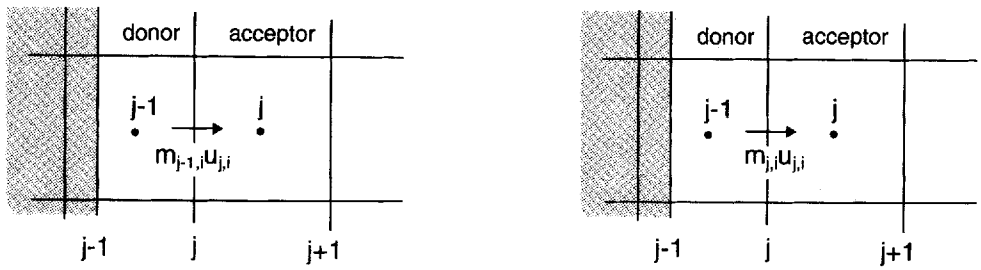

Figure 4. A schematic view of the numerical scheme (left: normal scheme, right: modified interfacial tracking scheme)

The interface tracking scheme may, when a front crosses a boundary, predict a negative specific mass of the transported 'emptying' fluid in the upstream cell, as well as too much of the other phase ($\alpha_1 < 0{\cdot}0$, $\alpha_2 > 1{\cdot}0$ and $\alpha_1 + \alpha_2 = 1{\cdot}0$). These 'extra' masses are readily corrected for as follows:

$$\begin{aligned} m_1^* &= \alpha_{1,j-1,i}\rho_{1,j-1,i}, & m_2^* &= (1-\alpha_{2,j-1,i})\rho_{2,j-1,i} \\ m_{1,j,i} &= m_{1,j,i} + m_1^*, & m_{2,j,i} &= m_{2,j,i} + m_2^*. \end{aligned} \tag{15}$$

3. RESULTS

3.1. Propagation of a single Taylor bubble in horizontal and inclined channels

The propagation of elongated bubbles in channels initially filled with liquid, closed at one end and open to the atmosphere at the other, has been simulated. The fluids applied were water and air, as indicated in Figure 5.

For horizontal channels Benjamin[9] obtained an analytical solution of the bubble propagation velocity, applying Bernoulli's theorem along the bubble surface.

$$u_b = 0{\cdot}5\sqrt{(gH)}, \tag{16}$$

where H is the channel height.

Applying the model of Moe and Bendiksen,[3] the effect of different constant interfacial friction factors [equation (9)] on the propagation velocity was investigated. The interfacial friction factor across the channel was set constant and equal to 10^{-3} in all simulations. The friction factor in the propagation direction is the free parameter in this study, and starting at a value of 10, it was increased until the velocity of the bubble converged to a constant value. The interface tracking scheme was not applied and the contour of the bubble was taken to be where the volume fraction is 0·5.

For low interfacial friction factors a considerable local slip between the phases results, whereas high values yield no slip between the phases. The results are shown in Figure 6, where the bubble velocity is calculated for a horizontal channel of $H = 0{\cdot}70$ m. The slip also determines the diffusion between the phases, as may be seen from Figure 7.

The applied time step has been limited by the Courant criterion as discussed by Moe and Bendiksen:[3]

$$\Delta t < \min\left(\frac{\Delta x_j}{u}, \frac{\Delta y_i}{v}\right) \tag{17}$$

where u and v are characteristic phase velocities in the x- and y-direction, respectively. The influence of the time step on the bubble velocity has been investigated. Seven nodes were used over the channel height and the same mesh size was applied along the channel.

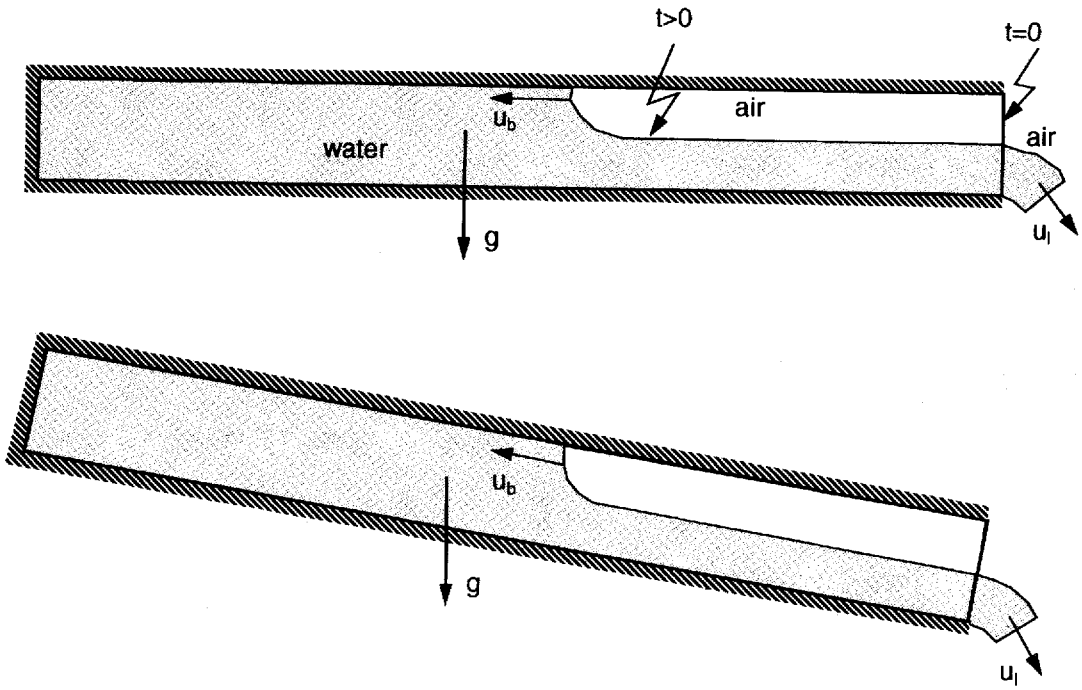

Figure 5. Propagation of elongated bubbles in horizontal and inclined channels. (upper: horizontal channel, lower: inclined channel)

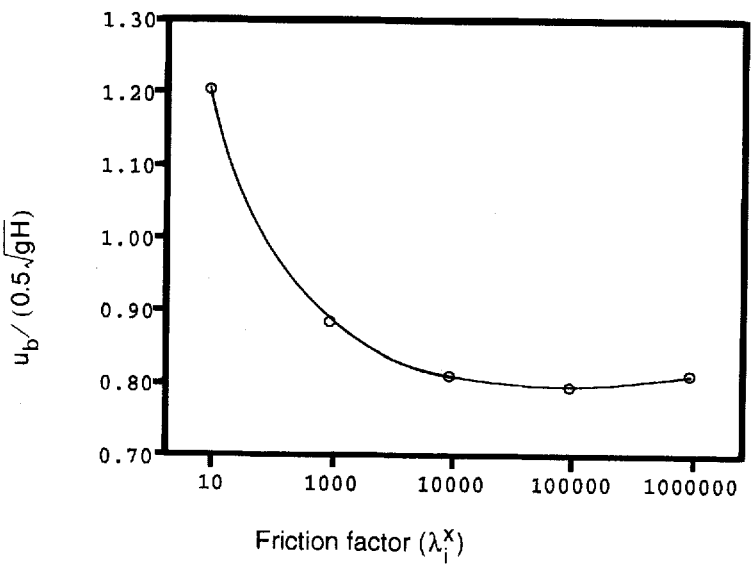

Figure 6. Effect of interfacial friction factor on dimensionless bubble propagation velocity

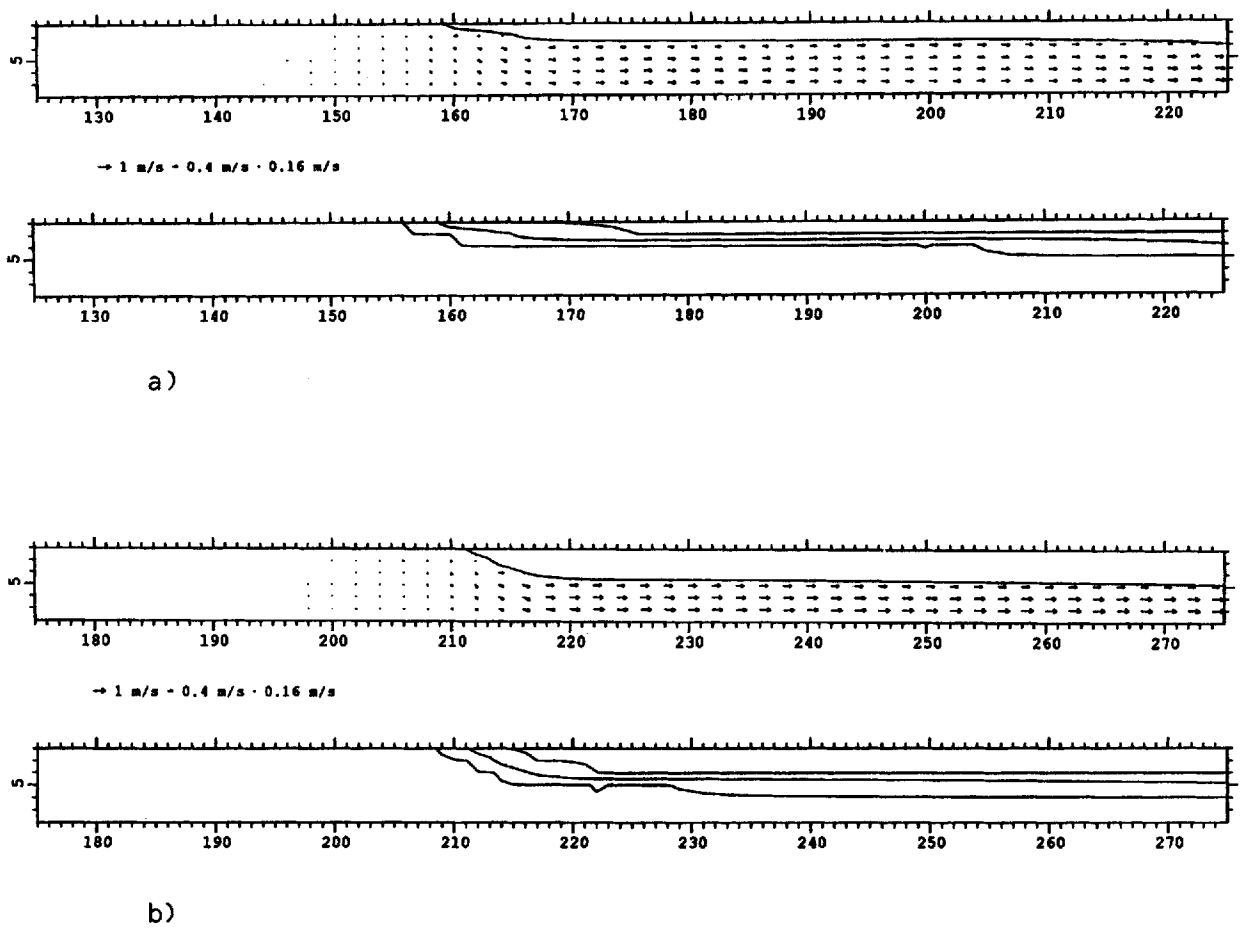

Figure 7. The calculated bubble shape for two different interfacial friction factors, (a) and (b), where the upper figure gives the liquid velocity profile and a contour of $\alpha = 0{\cdot}5$ and the lower one gives contours of $\alpha = 0$, 0·5, 1

The results are shown in Figure 8 for the three different models, two different interfacial friction models and the interface tracking model. The time step applied in the computations has very little effect on the bubble velocity for the interfacial tracking scheme and for interfacial friction model 2.

Interfacial friction model 1, equation (8), is a function of the volume fraction, giving friction factors in the range $0{\cdot}02 < \lambda_i^x, \lambda_i^y < 1{\cdot}52$. As seen from Figure 6, the bubble propagation velocity changes rapidly for low friction factors, which may explain the results of model 1 in Figure 8.

The effect of mesh size on the results was also investigated six, eight and ten nodes across the channel height were applied, with equal mesh size (node spacing) along the channel. Within the range of nodes tested, no significant influence on the bubble velocity was found for either model; see Figure 9.

A certain effect on bubble velocity was seen for non-uniform mesh size cases. The bubble velocity increases with increasing mesh ratio (between the mesh size in the x-direction and the mesh size in the y-direction) for all three models, as shown in Figure 10.

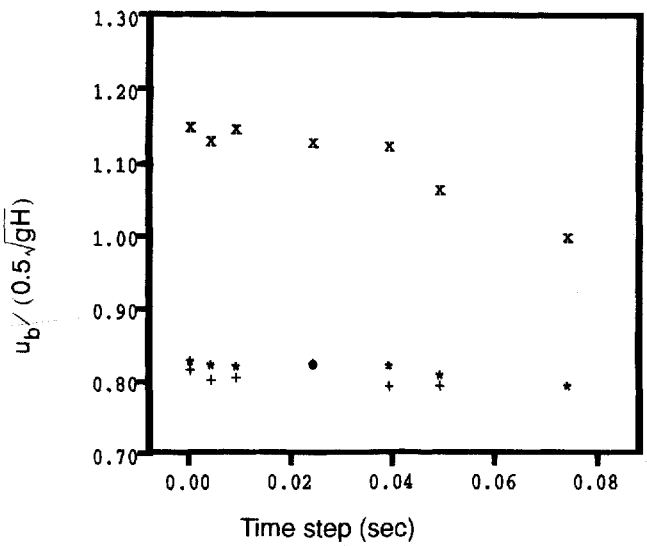

Figure 8. Dimensionless bubble velocity as a function of the applied time step (Interfacial friction: x model 1 (equation 8), * model 2 (equation 9), +Interface tracking)

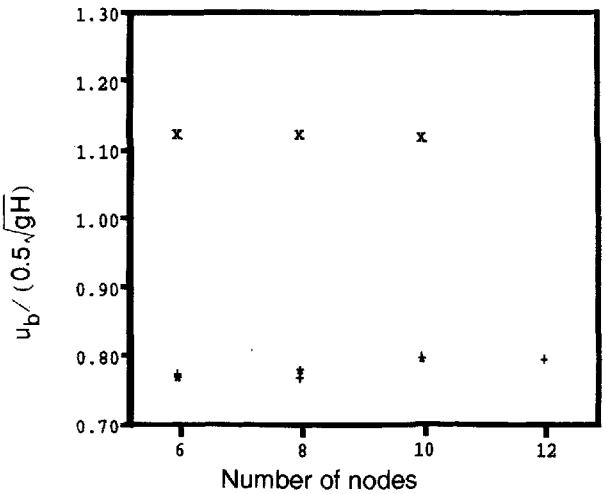

Figure 9. Dimensionless bubble velocity versus mesh size (given by the number of nodes across the channel height) (Interfacial friction: x model 1 (equation 8), * model 2 (equation 9), +Interface tracking)

Predicted bubble propagation velocities in horizontal channels of different heights were compared to the analytical solution of Benjamin [equation (16)] for all three models, as shown in Figure 11. All simulations were performed with seven nodes across the channel and time steps limited by the Courant criterion.

Interfacial friction model 1, which is of the Wallis type where λ_i is a function of liquid hold-up, again results in too high a diffusion of the bubble nose and therefore too large a bubble velocity. Interfacial friction model 2 and the interface tracking scheme give almost identical results for the bubble velocity, which, however, is too low compared to the analytical solution. The deviation from the analytical solution is limited to 20% for both models.

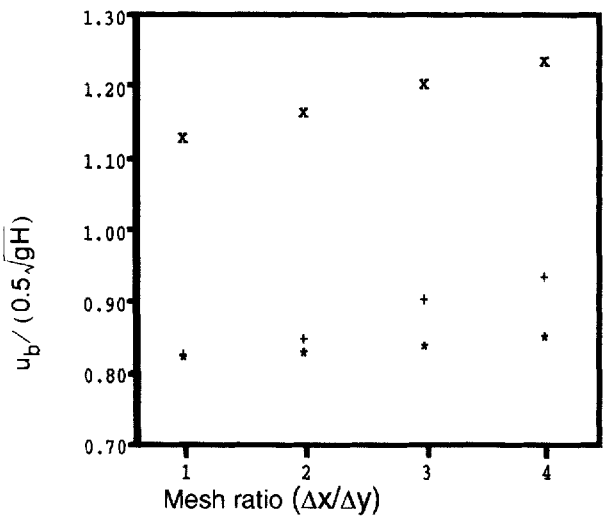

Figure 10. Dimensionless bubble velocity as a function of mesh ratios (Interfacial friction: x model 1 (equation 8), * model 2 (equation 9), +Interface tracking)

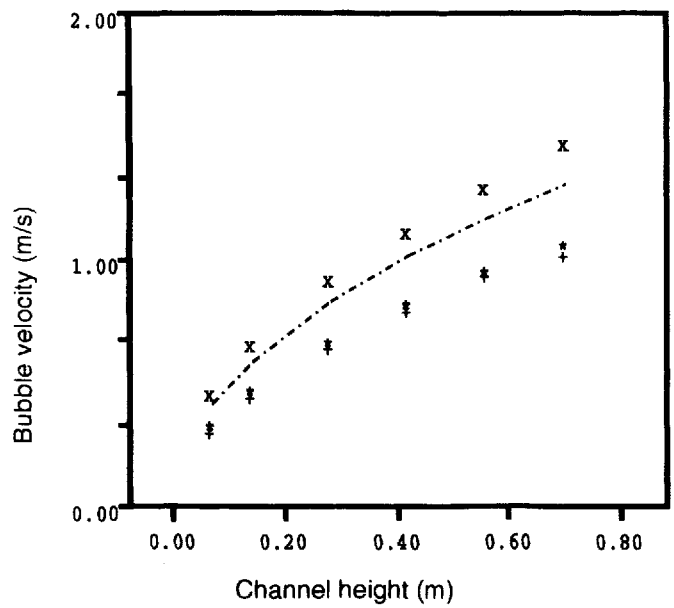

Figure 11. Bubble velocity in horizontal channels (Interfacial friction: x model 1 (equation 8), * model 2 (equation 9), + Interface tracking, -·- Analytical solution[9])

For inclined channels the discrepancies between the interfacial friction models become more pronounced. Two different channel inclinations, 5° and 15° with the horizontal, were simulated. The average dimensionless velocity for different channel heights are plotted against inclination in Figure 12. Again, it is seen that interfacial friction model 2 and the interfacial tracking scheme give almost identical results. It may also be concluded that the Wallis type of model for interfacial friction leads to very large numerical diffusion, and bubble velocities which are too great.

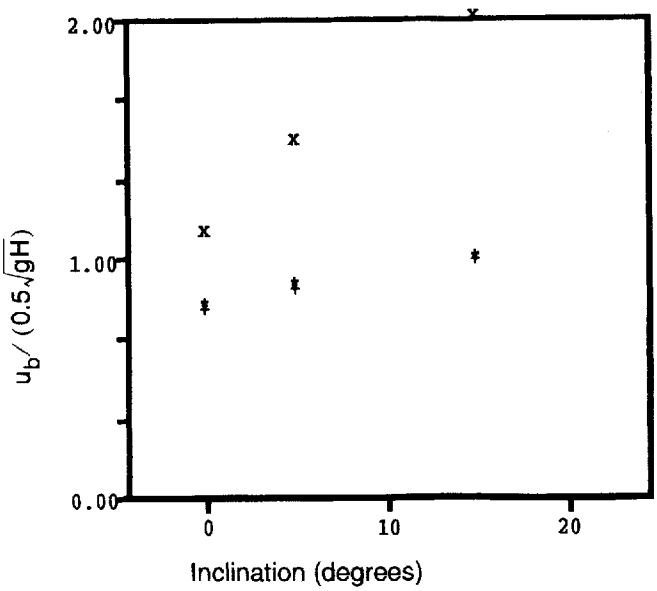

Figure 12. Dimensionless bubble propagation velocities in inclined channels (Interfacial friction: x model 1 (equation 8), * model 2 (equation 9), +Interface tracking)

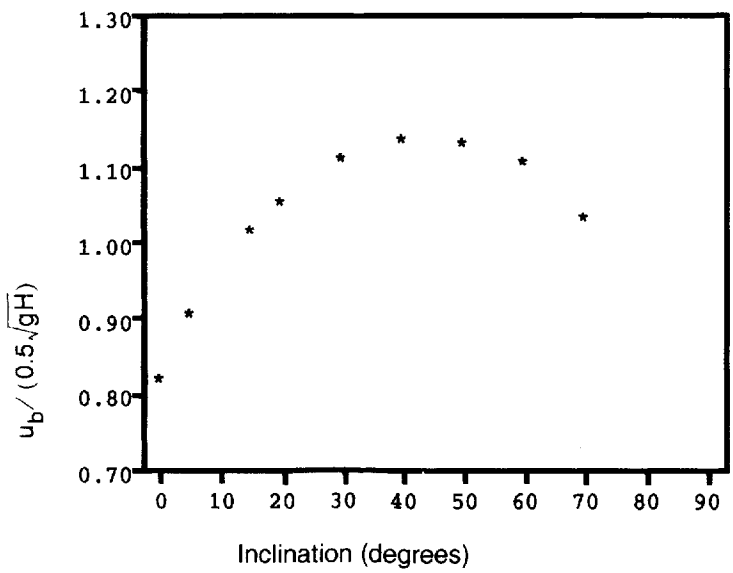

Figure 13. Dimensionless bubble propagation velocities in inclined channels using interfacial friction model 2

Having assessed that interfacial friction model 2 and the interfacial tracking scheme both give reasonable results for inclined channels, model 2 was used to simulate a wider range of channel inclinations up to 70° with the horizontal. Predicted dimensionless bubble propagation velocities are shown in Figure 13.

The bubble propagation velocity in circulr pipes has been measured by Zukoski[10] for inclinations between horizontal and vertical. The experimental results are shown in Figure 14 for air and water, for the case where surface tension effects are negligible ($\Sigma = 0{\cdot}001$, $\Sigma = 4\sigma/g\rho D^2$).

The predicted results for channels (Figure 13) seem to be qualitatively in reasonable agreement with the experimental results for pipes (Figure 14).

Influence of viscosity. In the work by Zukoski[10] the influence of viscosity on bubble propagation velocity was studied. For surface tension parameters Σ less than 0·5, the bubble velocity was found experimentally to depend on Reynolds number and Σ as

$$W_b(Re, \Sigma) = W_b(\infty, \Sigma) f(Re). \tag{18}$$

It was also concluded that the data presented in Figure 15 clearly fall into a high-Reynolds-number region, Re > 100, where $f(Re) \approx 1$ and a low-Reynolds-number region, $Re < 4$, where

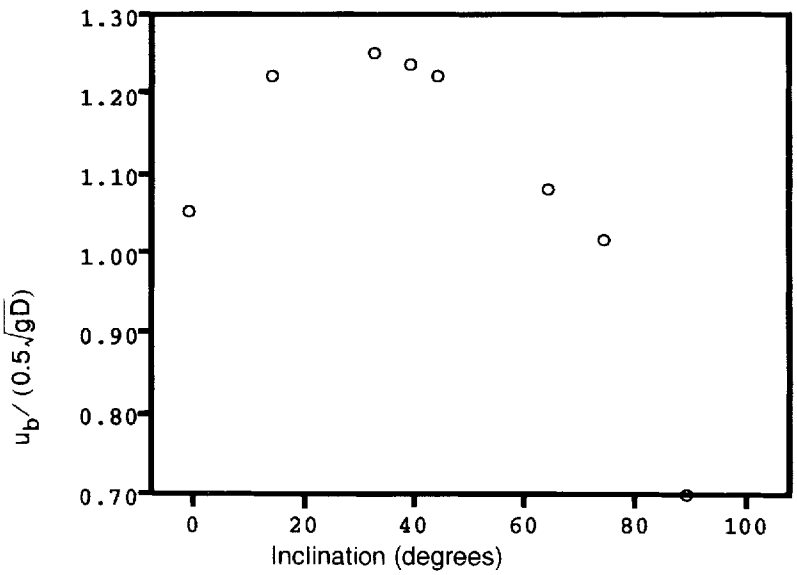

Figure 14. Dimensionless bubble propagation velocity in circular pipes, determined experimentally by Zukoski[10]

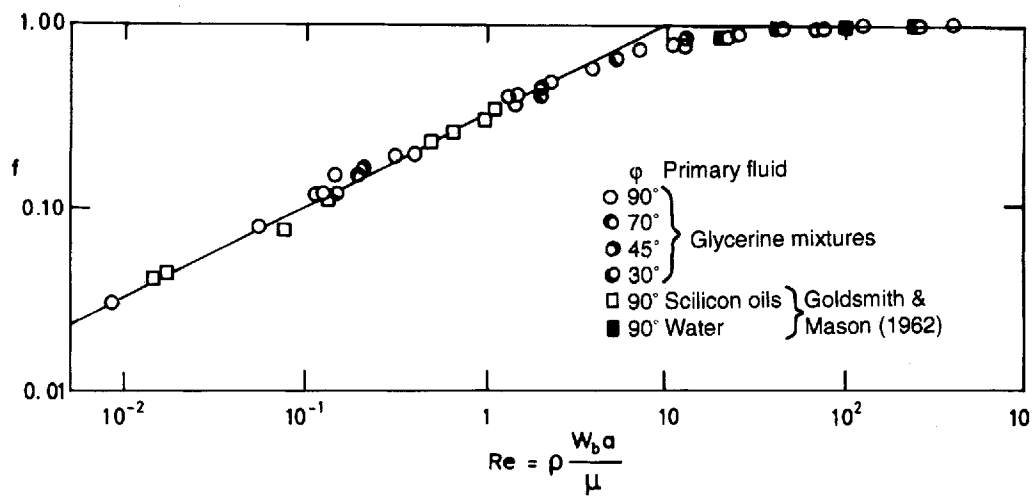

Figure 15. Influence of Reynolds number (viscosity) on the bubble propagation velocity $f = W_b(Re, \Sigma)/W_b(\infty, \Sigma)$, where W_b is the bubble propagation velocity (Zukoski[10])

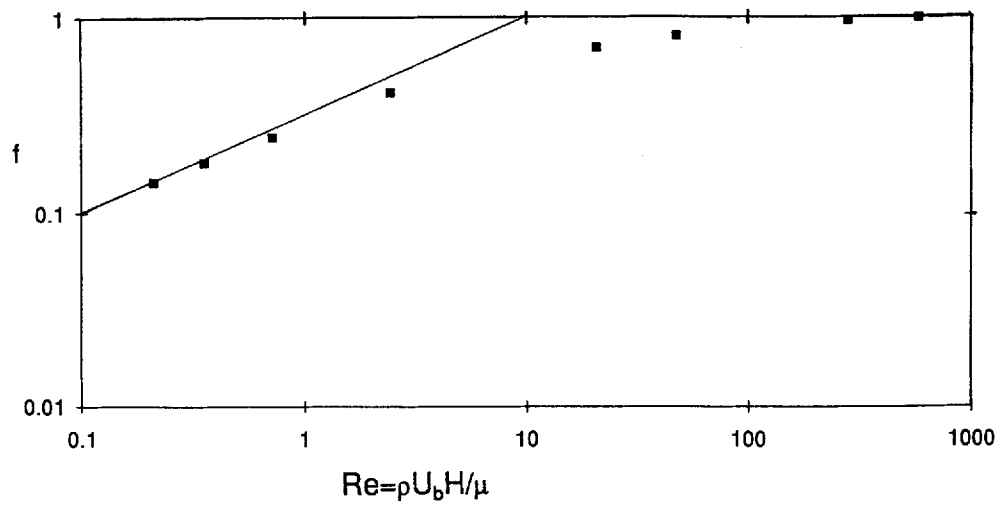

Figure 16. Predicted bubble propagation velocity in a 30° inclined channel for low Reynolds numbers $f = U_b(Re)/U_b(\infty)$, where U_b is the bubble propagation velocity

$f(Re) < 1$. The data show that the value of f is independent of the tube inclination for $30° \leq \varphi \leq 90°$.

In the present model, surface tension is neglected, but viscosity may be increased to simulate the influence of low Reynolds numbers. A channel of height 0·07 m with an inclination of 30° was selected as test case. Ten nodes were used across the channel and the same mesh size was applied in the axial direction. The time step was limited by the Courant criterion, and the channel was long enough to give a steady bubble motion. Interfacial friction model 2 [equation (9)] was used in the calculations. The computational results are given in Figure 16 and agree very well with the data of Zukoski for circular pipes.

3.2. Taylor bubble motion in downwardly-inclined channels

An extensive experimental study of the motion of long bubbles in inclined tubes was performed by Bendiksen,[1] For all inclinations and velocity regions, he concluded that the experimental data were well represented by

$$U_b = C_0 U_\ell + v_0, \tag{19}$$

where C_0 and v_0 are dependent on the Reynolds and Froude numbers, as well as on surface tension and pipe inclination. In particular, he observed that in downwardly inclined pipes the bubble turned relative to the liquid flow at a critical liquid flow rate.

Again, a channel of height 0·07 m was simulated with 10 nodes across the channel. A laminar velocity profile was imposed at the inlet for different flow rates. The bubble was given an initial idealized shape, as indicated in Figure 17. When the bubble propagates counter-currently against the liquid, as in the example shown, some of the initial gas volume is lost to the outlet surroundings during the first few time steps. Interfacial friction model 2 was again applied.

The bubble velocities were computed for three different inclination angles, $-2°$, $-5°$ and $-10°$, in a range of liquid velocities $0{\cdot}0 \leq u_\ell \leq 4{\cdot}0$ m/s. The results are shown in Figures 18–20.

For all three inclinations the predicted bubble velocities fall within three distinct regions. The first one, for the lowest liquid velocities, corresponds to the region where Bendiksen[11] found the bubble nose pointing against the liquid velocity, and where both $C_0 < 1$ and $v_0 < 0$.

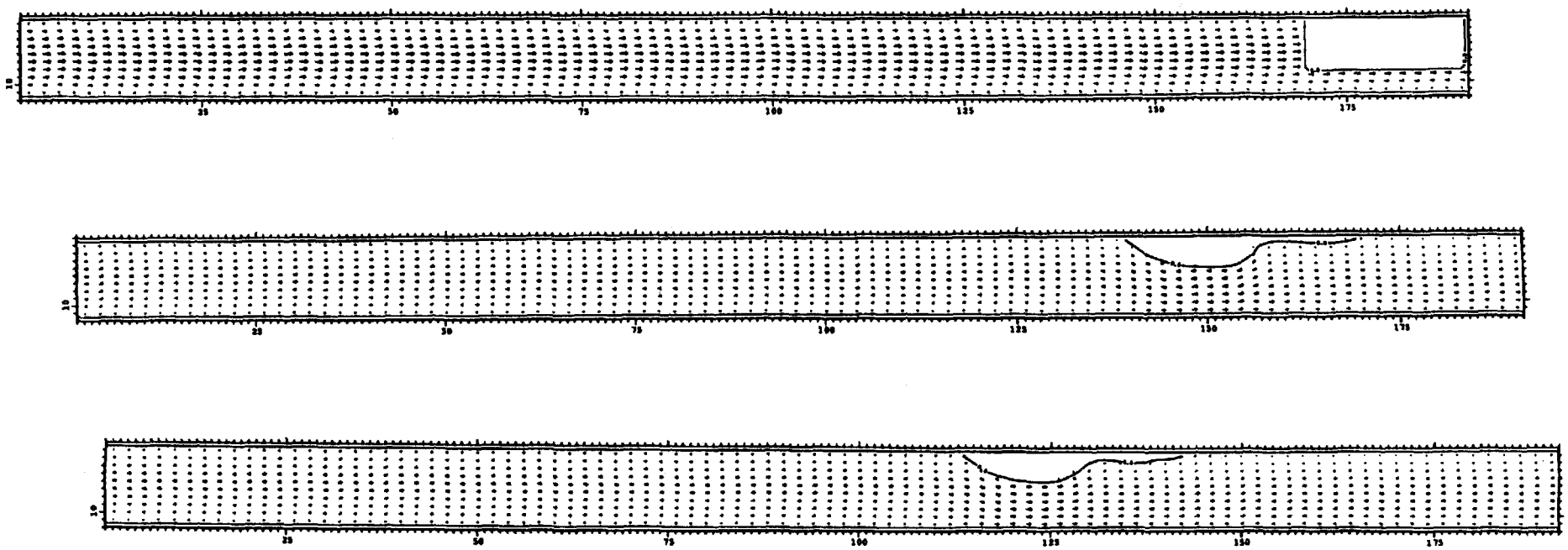

Figure 17. Bubble shapes at $t = 0{\cdot}0$, $1{\cdot}0$, $2{\cdot}0$ s in a $0{\cdot}07$ m channel with a downward inclination of 10° and an inlet liquid velocity of $0{\cdot}3$ m/s (from the left-hand side)

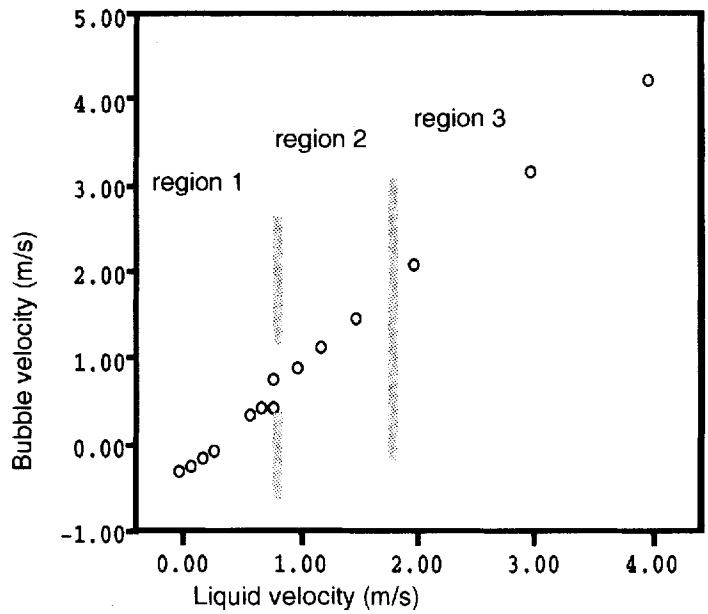

Figure 18. Predicted bubble velocity in a 7 cm high and 2° downwardly inclined channel

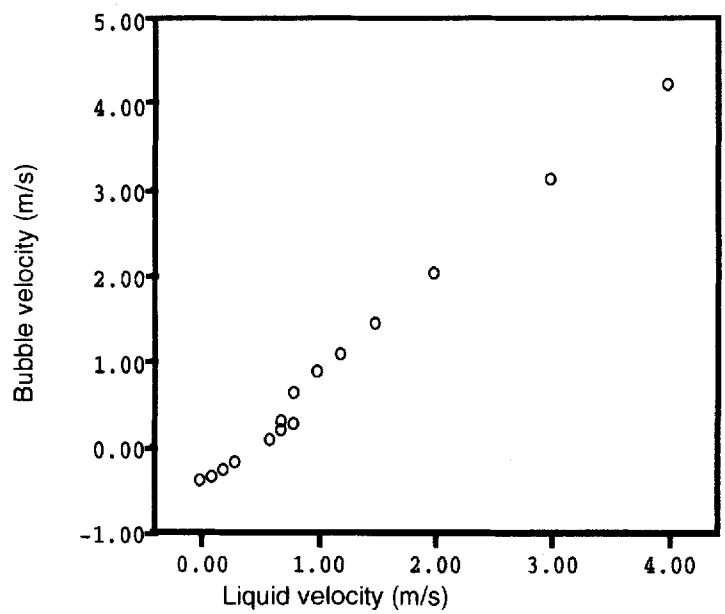

Figure 19. Predicted bubble velocity in a 7 cm high and 5° downwardly inclined channel

When the liquid velocity is increased, a critical velocity is obtained above which the bubble turns, and its motion is aligned with that of the liquid. At still higher liquid velocities (region 3, Figure 18), $C_0 > 1$ and $v_0 > 0$, and the bubble behaves much as in horizontal flow. The present model is not able to treat properly centred bubbles in a channel. However, it is clearly seen that

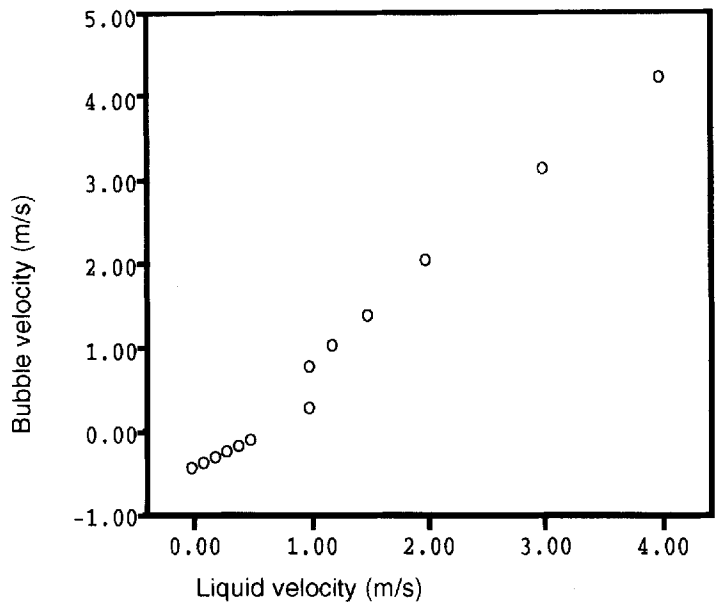

Figure 20. Predicted bubble velocity in a 7 cm high and 10° downwardly inclined channel

the liquid film below the bubble is decreased from region 1 to region 2, and that there is a corresponding sharp change in C_0, v_0 and thus in bubble velocity, as observed by Bendiksen.[11]

3.3. Taylor bubble shape in inclined channels

Finally, the powerful potential of this type of two-fluid models is demonstrated through a simulation of changes in Taylor bubble shapes with flow rate. At high liquid velocities in horizontal and inclined pipes, the tip of a large gas bubble will be increasingly centred. This gives $C_0 = 1{\cdot}2$ and $v_0 = 0$, as observed empirically by Bendiksen.[11] This is obviously a 3D effect where the tip of the bubble, e.g. in a horizontal pipe moves downwards due to the negative drift force caused by the parabolic local liquid velocity profile.

This may be seen from simulations of the motion of a gas bubble in a 2D channel with a downward inclination of 5° and a height 0·07 m. With an inlet liquid velocity, $u_\ell = 3$ m/s, it is apparent from Figure 21 that the gas bubble tends to move to the centre of the channel during the first time steps. However, the liquid film above the gas bubble is also influenced by the gravitational force, and starts to fall through the bubble, which then disintegrates. In an inclined pipe the liquid film around the bubble will instead start to move around the pipe wall, centring the bubble tip and keeping the bubble intact, as observed by Bendiksen.[11]

The simulations performed indicate, however, that the present physical model, although in a 3D version, would be a powerful tool in analysing these types of slug phenomena.

3.4. Initiation of slugs in upwardly inclined channels

The initiation of slug flow in upwardly inclined channels at fairly low gas and liquid flow rates has been simulated. Slugs form as a result of a very complicated liquid accumulation process, starting with the appearance of large waves giving increased interfacial friction and counteracting gravity.

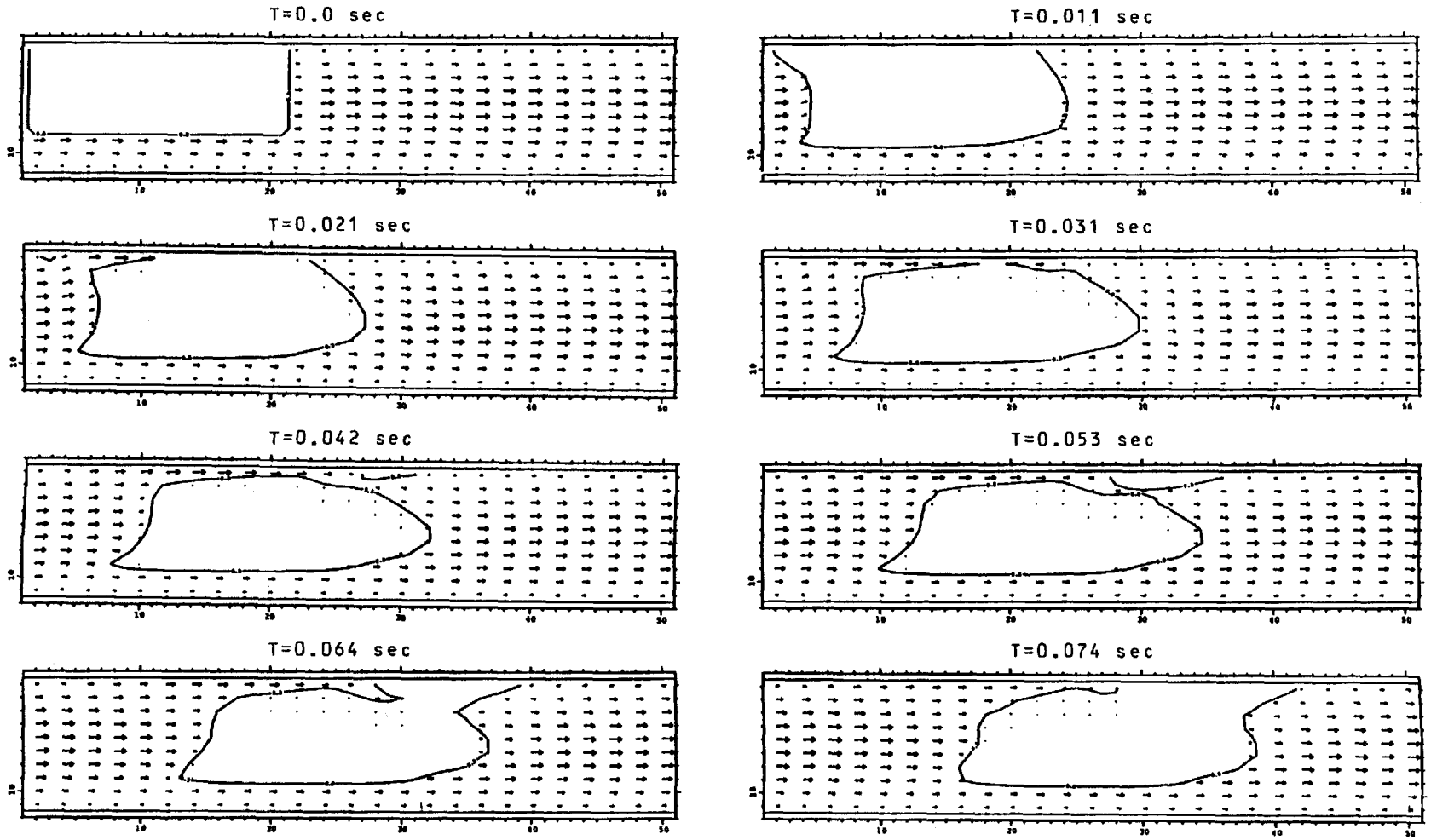

Figure 21. The evolution of a gas bubble at liquid velocity $u_r = 3{\cdot}0$ m/s in a channel of height $H = 0{\cdot}07$ m and downward inclintion of 5°

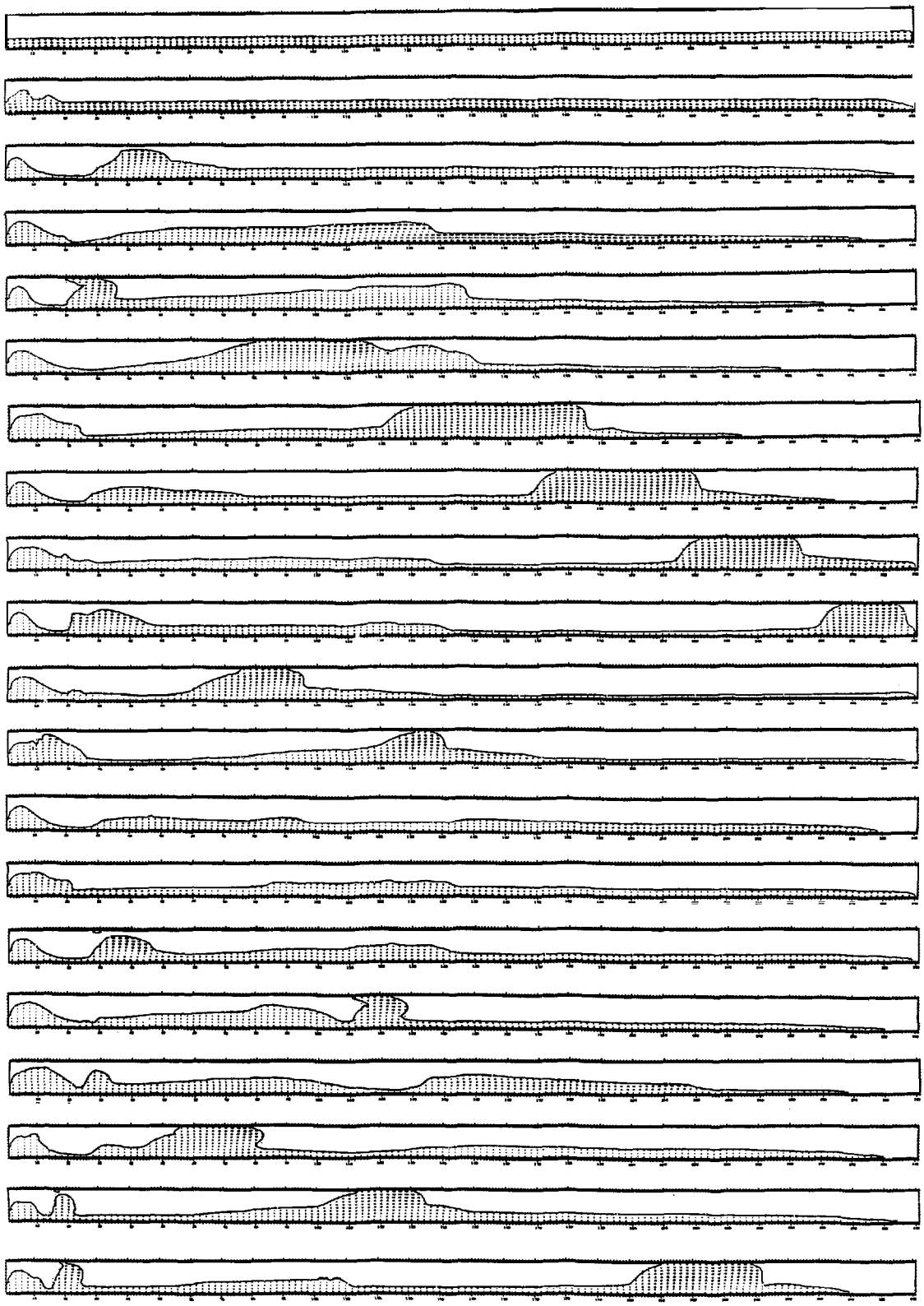

Figure 22. Initiation of slugs in an upwardly inclined channel of 20° and height 0·035 m

A channel of height 0·035 m and length 2·9 m with an inclination of 20° was simulated. Ten nodes were used across the channel and 290 in the axial direction, giving a mesh size ratio of nearly three. Again, interfacial friction model 2 was applied. The simulation started with a liquid film flow corresponding to a volume fraction of 30% with superficial velocities $U_{s\ell}=0{\cdot}15$ m/s and $U_{sg}=1{\cdot}4$ m/s ($U_{s\ell}=\alpha_\ell u_\ell$ and $U_{sg}=\alpha_g u_g$).

The results, presented in Figure 22, show several interesting phenomena characteristic of slug flow. As observed by Bendiksen and Espedal,[1,2] slugs are easily formed but do not always survive. A necessary condition for a given slug to grow is that it scoops up the liquid film in front of it at a larger rate than it sheds liquid at its tail. At the rather high inclination (20°) applied in the simulation, the effect of gravity on the liquid film is large. This results in an extremely non-steady dynamic type of flow, which is observed experimentally, but which also complicates direct comparisons with experimental data.

4. CONCLUSIONS

A new type of transient multidimensional two-fluid model[3] has been applied to simulate stratified and intermittent flows. The numerical method is based on a first-order semi-implicit finite difference scheme, and a direct two-step solution method, using a separate equation for the pressure. Two different types of interfacial friction models and an interfacial tracking scheme have been investigated. In general, the numerical scheme was found to be well suited to transient and intermittent flow analysis.

Simulation of Taylor bubble propagation in horizontal and inclined channels shows that the Wallis type of interfacial friction model gives large numerical diffusion at the interface, especially for inclined channels. The interfacial friction model 2, with no-slip conditions at the interfaces, gives less diffusion, and has been applied for stratified and intermittent flows. Further development of the interfacial friction model is required.

The proposed interfacial tracking scheme proved to be numerically stable and applicable to open Taylor bubbles. However, it gives very similar results to interfacial friction model 2, which is much simpler. In the case of bubble motion in downwardly inclined channels, the interfacial trackng scheme in its present form was numerically unstable. For bubbles not exposed to the atmosphere, a pressure correction over the interface, or more precisely within a cell containing the interface, is required.

Numerical diffusion of the interface was shown by Moe and Bendiksen[3] to depend also on the discretization of the convective terms in the momentum equations. The convective terms have been linearized in the present model, although the strongly accelerated flow field at the front and tail of a Taylor bubble makes this simplification questionable.

The results on Taylor bubble propagation in horizontal channels show satisfactory agreement with analytical solutions. Simulations in inclined channels predict the same trend for the bubble propagation as was observed experimentally in pipes. The same agreement holds for the effect of viscosity (low Reynolds number) on bubble propagation.

The bubble turning process in downflow illustrates the capability of the model to handle counter-current flow. At low rates a clear bubble nose shape is seen, pointing against the liquid flow. The model also predicts a critical velocity above which the bubbles turn and the motion is aligned with that of the liquid.

Initiation of slug flow in upwardly inclined channels has been simulated dynamically. The computations show, as observed experimentally, that slugs are easily formed but do not always survive.

ACKNOWLEDGEMENTS

The author wishes to thank Prof. K. H. Bendiksen for helpful discussions and support during this work. The author also gratefully acknowledges financial support from the PROFF program, under the Royal Norwegian Council for Scientific and Industrial Research (NTNF). Sponsoring participants are Total, Shell International Petroleum, Esso Norge a/s, Amoco Norway Oil Company, Elf Acquitane Norge a/s, Saga Petroleum a/s, Statoil, and Norsk Hydro a/s.

APPENDIX: NOMENCLATURE

A	area
a	pipe radius
D	pipe diameter
E	energy source
e	internal energy
f	function
$\mathbf{g}$	gravity (body force)
H	channel height
l_m	mixing length
$\mathbf{M}$	momentum source
$\mathbf{M}_m^R$	force due to change in mean curvature
m_k	specific mass, phase k ($m_k \equiv \alpha_k \rho_k$)
p	pressure
q	heat flux
r	radial co-ordinate
$R_{g/}$	mean curvature
Re	Reynolds number
$\mathbf{u}$	velocity
u	velocity, x-component
v	velocity, y-component
w	velocity, z-component
x, y, z	Cartesian co-ordinates

Greek letters

α	void fraction
Γ	mass transfer rate
φ	inclination
λ	bulk viscosity, friction factor
μ	viscosity
ν	kinematic viscosity
ρ	density
σ	surface tension
τ	stress tensor
$\Im$	unity tensor
$\wp$	stress tensor

Subscripts

g	gas phase
i	interface
i,j	directional indices
k	phase
m	mixture
ℓ	liquid phase

Superscripts

n	time index
T	turbulent
$'$	Fluctuating component
*	transposed (tensor)

REFERENCES

1. S. P. Antal, R. T. Lahey Jr. and J. E. Flaherty, 'Analysis of phase distribution in fully developed laminar bubbly two-phase flow', *Int. J. Multiphase Flow*, **17**, 635–652 (1991).
2. C. W. Hirt and B. D. Nichols, 'Volume of fluid (VOF) method for the dynamics of free boundaries', *J. Comput. Phys.*, **39**, 201 (1981).
3. R. Moe and K. H. Bendiksen, 'Transient simulation of 2–3D stratified and intermittent two-phase flows. part I. Theory', *Int. j. numer. methods fluids*, **16**, 461–487 (1993).
4. K. H. Bendiksen, D. Malnes, R. Moe and S. Nuland, *The Dynamic Two-Fluid Model OLGA: Theory and Application.* SPE Production Engineers, May 1991.
5. J. Liu and D. B. Spalding, 'Numerical simulation of flows with moving interfaces', *Physicochem. Hydrodyn.*, **10**, 625–637 (1988).
6. W. E. Johnson, 'Development and application of computer programs related to hypervelocity impact', *Systems Science and Software Report 3SR-353*, Los Alamos, 1970.
7. G. B. Wallis, *One-dimensional Two-phase Flow*, McGraw Hill, New York, 1969.
8. I. R. Ellull, 'The prediction of dispersed gas–liquid flow in complex pipe geometries, *Ph.D. Thesis*, Imperial College, London, 1989.
9. T. B. Benjamin, 'Gravity currents and related phenomena', *J. Fluid Mech.*, **31**, 209–248 (1968).
10. E. E. Zukoski, 'Influence of viscosity, surface tension, and inclination angle on motion of long bubbles in closed tubes', *J. Fluid Mech.*, **25**, 821–837 (1966).
11. K. H. Bendiksen, 'An exprimental investigation of the motion of long bubbles in inclined tubes', *Int. J. Multipnase Flow*, **10**, 467–483 (1984).
12. K. H. Bendiksen and M. Espedal, 'Onset of slugging in horizontal gas–liquid pipe flow', *Int. J. Multiphase Flow*, **18**, 237–247 (1992).
13. K. H. Bendiksen, D. Malnes, T. Straume and P. Hedne, 'A non-diffusive numerical model for transient simulation of oil-gas transportation systems', *Proc. 1990 European Simulation Multiconference*, 1990, pp. 508–515.